



Past and present seafloor age distributions and the temporal evolution of plate tectonic heat transport

Thorsten W. Becker^{a,*}, Clinton P. Conrad^b, Bruce Buffett^c, R. Dietmar Müller^d

^a Department of Earth Sciences, University of Southern California, Los Angeles, CA, USA

^b Department of Geology and Geophysics, SOEST, University of Hawaii, Honolulu HI, USA

^c University of California at Berkeley, Berkeley CA, USA

^d EarthByte Group, School of Geosciences, University of Sydney, Sydney NSW, Australia

ARTICLE INFO

Article history:

Received 29 September 2008

Received in revised form 2 December 2008

Accepted 2 December 2008

Available online 21 January 2009

Editor: R.D. van der Hilst

Keywords:

seafloor age distributions

plate tectonics

oceanic heat flow

ABSTRACT

Variations in Earth's rates of seafloor generation and recycling have far-reaching consequences for sea level, ocean chemistry, and climate. However, there is little agreement on the correct parameterization for the time-dependent evolution of plate motions. A strong constraint is given by seafloor age distributions, which are affected by variations in average spreading rate, ridge length, and the age distribution of seafloor being removed by subduction. Using a simplified evolution model, we explore which physical parameterizations of these quantities are compatible with broad trends in the area per seafloor age statistics for the present-day and back to 140 Ma from paleo-age reconstructions. We show that a probability of subduction based on plate buoyancy (slab-pull, or "sqrt(age)") and a time-varying spreading rate fits the observed age distributions as well as, or better than, a subduction probability consistent with an unvarying "triangular" age distribution and age-independent destruction of ocean floor. Instead, we interpret the present near-triangular distribution of ages as a snapshot of a transient state of the evolving oceanic plate system. Current seafloor ages still contain hints of a ~60 Myr periodicity in seafloor production, and using paleoages, we find that a ~250 Myr period variation is consistent with geologically-based reconstructions of production rate variations. These long-period variations also imply a decrease of oceanic heat flow by ~-0.25%/Ma during the last 140 Ma, caused by a 25–50% decrease in the rate of seafloor production. Our study offers an improved understanding of the non-uniformitarian evolution of plate tectonics and the interplay between continental cycles and the self-organization of the oceanic plates.

© 2008 Elsevier B.V. All rights reserved.

1. Introduction

Earth's heat loss over geologic times is mainly controlled by the motions of the oceanic lithosphere. The continuously recycled oceanic plates form the surface boundary layer for mantle convection, and the efficiency of plate tectonics in transporting heat is reflected in spreading and subduction rate variations. Such fluctuations not only control Earth's thermal evolution but also affect relative sealevel, climate, and ocean geochemistry (Larson and Pitman, 1972; Hays and Pitman, 1973; Parsons, 1982). Most of those processes are linked to the variations of the global seafloor age distribution, on which we focus here. Specific events, such as the association between high spreading rates and the Cretaceous sealevel high-stand, are debated (e.g. Heller et al., 1996). However, plate tectonic variability is consistent with observations of fluctuating seawater chemistry (Hardie, 1996) and sealevel (Gaffin, 1987), and is also expected from spherical convection models (e.g.

Phillips and Bunge, 2005; Zhong et al., 2007; Walzer and Hendel, 2008). Heat flow variations may arise, for example, from changes in the aspect ratios of convective cells (Grigné et al., 2005). Loyd et al. (2007) used reconstructed, "paleo" ages to show that heat flow has likely decreased at a rate of ~-0.2%/Ma over the last 60 Ma. The finding that heat flow is relatively low at present, rather than high as suggested by Grigné et al. (2005), is consistent with Korenaga's (2007) argument based on sealevel variations, earlier heat flow estimates based on seafloor age (Harrison, 1980), and new estimates made below using the paleo ages from Müller et al. (2008b) (hereafter: M08) back to 140 Ma. Smaller amplitudes of variations as estimated by Korenaga (2007) may be caused by the difficulty of using sea level to constrain oceanic tectonics because observations are region-dependent and corrections are needed due to dynamic topography (e.g. Gurnis, 1990; Lithgow-Bertelloni and Gurnis, 1997). This speaks to the ambiguity in using individual observations such as sealevel as constraints. However, the consistency between sea level and heat flow variability was interpreted by both Loyd et al. (2007) and Korenaga (2007) as evidence for episodic, or punctuated, fluctuations in plate tectonics and convection.

It is crucial to integrate a range of observables into evolutionary models of heat transport variations. The most important constraint

* Corresponding author. Department of Earth Sciences, University of Southern California, MC 0740, 3651 Trousdale Pkwy, Los Angeles, CA 90089-0740, USA. Tel.: +1 213 740 8365; fax: +1 213 740 8801.

E-mail address: twb@usc.edu (T.W. Becker).

comes from the seafloor age distribution (e.g. Sclater et al., 1981; Parsons, 1982; Müller et al., 1997, 2008a). For the present-day, $t=0$, the distribution of seafloor area per unit age, $\alpha(\tau, t)$, for age τ is well constrained and can be fit by

$$\alpha(\tau, t=0) \approx C_0(1-\tau/\tau_m) \quad \text{“ triangular distribution ”} \quad (1)$$

where the seafloor production rate $C_0 \sim 3 \text{ km}^2/\text{yr}$, and the maximum seafloor age $\tau_m \sim 180 \text{ Myr}$ (Parsons, 1982; Rowley, 2002; Cogne and Humler, 2004). Rowley (2002) argues that the simplest explanation for the observed age distribution is that the seafloor production rate and the maximum seafloor age have been constant throughout the last 180 Ma. This implies that the rate of seafloor destruction is independent of seafloor age (Parsons, 1982), which is unlike what simple models predict. For example, the negative buoyancy of slab pull increases with $\tau^{1/2}$ from thermal boundary layer analysis. All material with τ larger than a cutoff age, τ_c , should then subduct once viscous effects, perhaps complicated by compositional buoyancy (e.g. Davies, 1992), are overcome. Such behavior will lead to preferential subduction of older seafloor and is seen in thermal convection computations (e.g. Labrosse and Jaupart, 2007).

Clearly, we expect the lithosphere to behave differently from a simple convective boundary layer. In terms of rheology, the viscous dissipation due to plate bending in subduction zones may be important (Conrad and Hager, 1999; Becker et al., 1999), making old plates less likely to subduct than expected from their negative buoyancy. Due to the feedback between heat transport and mantle temperature, there will also be an effect on melting at ridges, and resulting dehydration stiffening of the oceanic plate (e.g. Lee et al., 2005; Korenaga, 2008). Rheological complexities aside, tectonics on a sphere requires ridge-trench triple junctions where zero age seafloor subducts (Rowley, 2002), and the geometrical effects of continents overriding subducting oceanic plates will also matter (Labrosse and Jaupart, 2007). What is not clear is how important those effects are, and how significant the current distribution of seafloor ages is for the long-term evolution.

On one hand, the triangular shape of the age distribution at present, $\alpha(t=0)$, may be special and place fundamental constraints on tectonics (Rowley, 2002). Triangularity may then also contain an empirical description of the physics that can be incorporated into parameterized convection studies (Labrosse and Jaupart, 2007). Alternatively, $\alpha(t=0)$ can be considered as the firmest among several constraints on mantle evolution while allowing for the possibility that there are numerous potential paths, including those with large degrees of production rate variation, that may have led to the current age distribution. Demicco (2004) provided a stochastic model illustrating such non-uniqueness; we build on this work and test several, physically-motivated subduction probabilities in a one-dimensional seafloor age evolution model.

Part of this debate is related to the significance of variations in seafloor production rate associated with deviations from the triangular distribution (Rowley, 2002; Cogne and Humler, 2004; Conrad and Lithgow-Bertelloni, 2007; Müller et al., 2008a). Another aspect is whether uniformitarian constancy, or non-uniform fluctuations in spreading rates and ridge length are considered as a simpler explanation of the data. We attempt to address these issues by integrating the age distribution through time and comparing to age distributions for the present and inferred from reconstructions. We find that a physical model where subduction probability is proportional to the square root of plate age, but seafloor creation rates are allowed to vary, provides an alternative description of the present-day, cumulative seafloor age distribution.

2. A one-dimensional model of seafloor age

Sphericity imposes constraints on plate kinematics such as the degree of toroidal motions (Olson and Bercovici, 1991; O’Connell et al.,

1991) and will also leave an imprint in area per age distributions, α , particularly in the presence of continental plates (Labrosse and Jaupart, 2007). A spherical, multi-plate system is cumbersome to analyze, which is why we focus on a simplified model. We assume constant total oceanic plate area, Σ_0 ,

$$\Sigma_0 = \int_0^\infty \alpha(\tau, t) d\tau. \quad (2)$$

At least for the Cenozoic, this assumption should be justified (Cogne and Humler, 2004; Xu et al., 2006). In our model, changes in the seafloor age distribution with age and time increment $d\tau$ and dt , respectively, are governed by subduction such that

$$\alpha(\tau + d\tau, t + dt) = \alpha(\tau, t) - \Phi(\tau, t) dt, \quad (3)$$

where $\Phi(\tau, t)$ is the rate of seafloor destruction (using a positive sign for subduction). Eq. (3) is the solution of the governing differential equation

$$\frac{\partial \alpha}{\partial \tau} + \frac{\partial \alpha}{\partial t} = -\Phi(\tau, t) \quad (4)$$

by the method of characteristics, i.e. Eq. (3) expresses the evolution of seafloor age along different paths as determined by the boundary condition $\alpha(\tau=0, t) = C(t)$, where $C(t)$ is the seafloor production rate at the (zero-age) spreading centers.

Complexities of plate dynamics and continental cover will be incorporated in the subduction rate Φ if they lead to a temporally averaged modification of the system. Fluctuations from the average behavior, such as those due to regional plate reorganizations, will lead to deviations from the model predictions for α . Assuming that the rules that govern subduction are not time-dependent, Φ can be written as the product of the area per age of seafloor that is available for subduction and an age-dependent subduction probability ϕ

$$\Phi(\tau, t) = \alpha(\tau, t) \phi(\tau). \quad (5)$$

For Eq. (2) to hold, seafloor production at zero age has to balance the age-integrated destruction at all times,

$$C(t) = \int_0^\infty \Phi(\tau, t) d\tau. \quad (6)$$

Eq. (6) can be obtained from Eqs. (2) and (4) by integration over age with the requirement $\alpha(\tau=\infty)=0$, and allows a numerical evaluation of Eq. (3) for different $C(t)$ and ϕ scenarios. Numerically, we use $d\tau=dt=0.5 \text{ Ma}$ to advance the solution.

We consider both geologically motivated variations in production rate and periodic variations around a reference production rate C_0 ,

$$\frac{C(t)}{C_0} = A_0 + \sum_{i=1}^{n_h} A_i \cos(\omega_i t + \gamma_i), \quad (7)$$

where A_0 differentiates the long-term averaged rate from the present C_0 . Up to two harmonics ($n_h=2$) are used with periods $T_i=2\pi/\omega_i$. When inverting for best-fit $C(t)$ models, we constrain the phases γ_i such that $C(t=0)=C_0$, and also require $0.1 < C(t)/C_0 < 5$, $0 < T_i < 1000 \text{ Myr}$, and $0 \leq A_{1,2} \leq 0.5$ to reduce non-uniqueness while the misfit between predicted and observed age distribution is minimized by a Simplex scheme (Nelder and Mead, 1965). These parameter ranges are motivated by the geologically constrained scenarios discussed below.

2.1. Subduction probability models

In order to explore the parameter space, we consider five subduction probability models, ϕ , and their corresponding steady-state area per age distributions, α^{ss} , for constant C_0 as shown in Fig. 1.

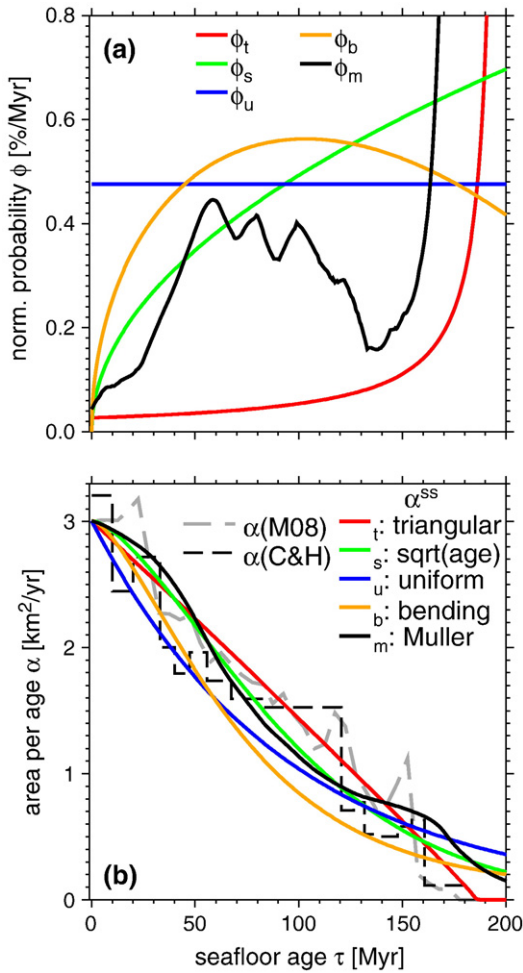


Fig. 1. (a) Subduction probabilities $\phi(\tau)$ for different models, normalized for plotting purposes such that $\int_0^{210} d\tau = 1$. (b) Steady-state area per age solutions, α^{ss} , for fixed production rate of $C_0 = 3.0$ km²/yr and the probabilities of (a). Dashed lines show present-day $\alpha(t=0)$ based on M08 (gray) and from Cogne and Humler (2004) (black).

2.1.1. Triangular probability

For the constant seafloor production scenario and uniform subduction rate ($\phi=c$, with $c>0$ constant for $\tau<\tau_m$, and zero otherwise), the steady-state area per age, α_t^{ss} , is given by the triangular distribution, Eq. (1) (Parsons, 1982). Further, if Eq. (5) holds, constant $\phi=c$ implies (from Eq. (4)) that

$$\phi_t = \frac{1}{\tau_m - \tau}. \quad (8)$$

This means that strict triangularity for the age distribution α at constant destruction rate ϕ leads to a non-zero probability of subduction at zero age, $\phi_t(0)>0$, as required by ridge-trench triple junctions, but also a seemingly unphysical behavior for ϕ_t as $\tau \rightarrow \tau_m$ (Fig. 1a; numerically, we set ϕ_t to unity for $\tau \geq \tau_m$).

2.1.2. Sqrt(age) probability

If slab pull is dominant, the subduction probability should be proportional to the square-root of seafloor age,

$$\phi_s = k_1 \tau^{1/2}, \quad (9)$$

where the factor k_1 is determined at each time step from Eq. (6). The steady-state solution for Eq. (9) at constant C_0 is $\alpha_s^{ss} = C_0 \exp(-2/3k_1\tau^{3/2})$ (from Eqs. (4) and (5)) and matched by the numerical solution shown in

Fig. 1b to within 1% for $\tau < 200$ Myr. In comparison to the triangular α_t^{ss} , α_s^{ss} predicts relatively less intermediate age seafloor, and small but non-zero α for all τ .

2.1.3. Uniform probability

If there is no dependency on age in the subduction probability itself, we can write

$$\phi_u = k_2, \quad (10)$$

where k_2 is computed from Eq. (6) as above. There are no inflection points for the corresponding α_u^{ss} since this solution is an exponential; the α_u^{ss} age per area distribution is smaller than α_t^{ss} or α_s^{ss} for $\tau < 120$ Myr (Fig. 1b).

2.1.4. Slab bending model

We can approximately account for the effect of plate bending at subduction zones following the derivation by Buffett (2006). Assuming that the plate thickness in the buoyancy and bending force (Eqs. (18) and (22) of Buffett, 2006, respectively) scales with $\tau^{1/2}$, and posing that the resulting subduction probability scales with the difference between the two, we can write

$$\phi_b = k_3 \tau^{1/2} - k_4 \tau^3, \quad (11)$$

with solution $\alpha_b^{ss} = C_0 \exp(-2/3k_3\tau^{3/2} + 6/15k_4\tau^{5/2})$ for $C=C_0$. (Numerically, we also require $\phi_b \geq 0$ for all τ , and set ϕ_b to a constant, small value for ages $\tau > 200$ Myr. Without this requirement, a very long tail for α results. Unlike other ϕ models, the results for ϕ_b therefore depend slightly on modeling details.)

The k_4 factor of the bending term that opposes the slab pull hides the product of $\eta u_0/R^3$ where R is the slab bending radius, η lithospheric viscosity, and u_0 plate velocity, all of which we assume to be constant. Those parameters are, of course, regionally variable on Earth, R evolves over time for dynamic models (Becker et al., 1999), and η will depend on the age of the plate at subduction. While this complicates the application of viscous slab bending theory to nature, those issues are less relevant here as we merely wish to contrast the sqrt(age) model with a bending approach that has a reduced likelihood of subduction at large ages. The ϕ_b probability used here (Fig. 1a) results from plausible choices such as instability/slab length 200 km, $R=220$ km, and $\eta=6 \times 10^{22}$ Pa s in which case $k_4/k_3 \approx 0.003$ Myr⁻¹, but should only be considered as an example. The resulting α_b^{ss} age distribution for this particular k_4/k_3 ratio leads to relatively low α_b^{ss} values at intermediate ages; the preferred subduction of intermediate τ seafloor also leads to a long “tail” and finite α for $\tau \rightarrow \infty$ (Fig. 1b).

2.1.5. Empirical Müller probability

Lastly, we consider the average subduction probability, ϕ_m , that is implied by the M08 paleo-age reconstructions. We estimate ϕ_m by dividing the area of subducted seafloor per 1 Ma interval in M08, Φ , by α (Eq. (5)), computing a geometric mean for the past 140 Ma, and smoothing results with a 10 Myr wide boxcar filter (Fig. 1a). This ϕ_m probability captures the effective evolution for seafloor age that is implicit in M08; ϕ_m is similar to ϕ_s for young ages, but non-zero at $\tau=0$, and relatively diminished for τ between 100 and 150 Myr. This leads to a local maximum in the α_m^{ss} curve at $\tau \sim 160$ Myr (Fig. 1b). The sharp increase in ϕ_m at ~ 160 Myr is due to division by small values of α , which leads to an unstable estimate of ϕ_m for $\tau > 170$ Myr. (Numerically, we use $\phi_m(\tau > 170 \text{ Myr}) = \phi_m(\tau = 170 \text{ Myr})$). Besides the large age spike, the bending, ϕ_b , model is most similar in shape to ϕ_m (Fig. 1a). Assuming M08 provides an adequate description of the seafloor age evolution, this provides a hint that oceanic plate dynamics may be affected by the bending of slabs, and the ϕ_b probability could perhaps be adjusted to match ϕ_m .

2.2. Quantities derived from seafloor age distributions

A given age distribution can be cast in terms of quantities that are relevant for Earth evolution including oceanic heat flow and sealevel. Following Loyd et al. (2007), we assume a modified half-space cooling law holds such that the total oceanic heat flow Q is given by

$$Q(t) = q_a \int_0^{80} \alpha(\tau, t) \tau^{-1/2} d\tau + q_b \int_{80}^{\infty} \alpha(\tau, t) d\tau, \quad (12)$$

where τ is in Myr, $q_a = 480 \text{ mW m}^{-2} \text{ Myr}^{-0.5}$, and $q_b = 48 \text{ mW m}^{-2}$ (Jaupart et al., 2007). For sealevel, we assume constant ocean volume, and compute the mean depth of the ocean floor, \bar{d} , from

$$\bar{d}(t) = \frac{1}{\Sigma_0} \int_0^{\infty} d(\tau) \alpha(\tau, t) d\tau, \quad (13)$$

where $d(\tau)$ is from the modified half-space model of Stein and Stein (1992). Relative sealevel, S , is then computed by isostatically compensating the deviations of \bar{d} from the present-day

$$S(t) = -(\bar{d}(t) - \bar{d}(0)) \left(1 - \frac{\rho_w}{\rho_m} \right). \quad (14)$$

Here, $\rho_w = 1000 \text{ kg/m}^3$, $\rho_m = 3300 \text{ kg/m}^3$, and we ignore complications, such as due to continental shelves (e.g. Pitman, 1978).

3. Paleo-age reconstructions

We have some knowledge of the actual spreading rate variations, for example from preserved anomalies in the present-day seafloor. However, any attempts to reconstruct global, long-term seafloor production rates will have inherent uncertainties because a large fraction of the seafloor has been removed. This is particularly true if reconstructions of seafloor age are attempted based on plate tectonic models. For estimates of paleo-ages at 50 Ma, ~50% of the seafloor needs to be reconstructed; going back to 140 Ma, the situation is even more severe, and ~90% of the seafloor has to be model-based (Xu et al., 2006; Müller et al., 2008b).

There are two, related types of errors for paleo-ages: those that are due to uncertainties in the plate tectonic reconstructions, and those due to uncertainties in past spreading rates. How different tectonic reconstructions in the western Pacific, for example, affect such inferences is discussed by Xu et al. (2006) and Loyd et al. (2007). For times older than 60 Ma, M08's reconstructions differ from those of Engebretson et al. (1985), e.g. when treating the Izanagi plate. This explains some of the discrepancies of our study with previous work; Loyd et al. (2007) based their analysis on older reconstructions (Engebretson et al., 1985; Lithgow-Bertelloni et al., 1993).

Reconstructions of spreading rates are also dependent on the geological time-scale used, particularly during the Cretaceous (e.g. Fiet et al., 2006). Uncertainties in the amplitude and symmetry of spreading will make the region of young seafloor close to the ridge narrower or wider. For our use of M08, we experimented with several error estimates and chose a somewhat arbitrary approach that is, however, guided by our attempt to provide conservative error estimates. We use the age uncertainty maps provided by M08, σ^{M08} , as a basis. Then, we compute a maximum error by considering the full range of $\tau \pm \sigma^s$ for error bars on τ and derived quantities such as α . To compute this adjusted error, σ^s , we scale σ^{M08} such that the error decreases toward the ridges so that the geographic regions with age $\tau \approx 0$ are preserved when adding or subtracting $\tau \pm \sigma^s$:

$$\sigma^s = \sigma^{\text{M08}} (\tau / \tau_s) \text{ for } \tau \leq \tau_s, \text{ and } \sigma^s = \sigma^{\text{M08}} \text{ otherwise.} \quad (15)$$

The scale age τ_s was chosen as 30 Myr to avoid negative ages for smaller τ_s , which lead to disappearing ridges for the lower error bound. When computing α from M08 paleo-ages (Fig. 2), the maximum error

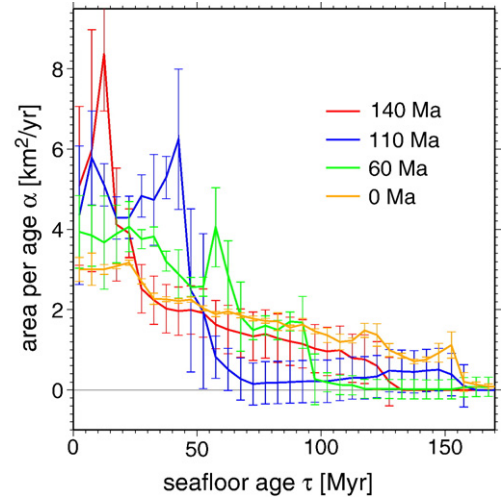


Fig. 2. Global area per age distributions computed by 5 Myr binning of the paleo seafloor age reconstruction of Müller et al. (2008b), with uncertainties computed from maximum error estimates for paleo-age.

approach leads to small uncertainties in the large τ , small α tail of these age distributions. We consider this an artifact because much of the oldest seafloor will have been extrapolated. We therefore enforce uncertainties on $\alpha(\tau)$ for $\tau > 180 - t$ to be at least 50% of the mean of the larger uncertainties of the younger part of the α curve. Our inferences on heat flow and time-variability of convection based on M08 will consider these error bounds, and it is clear that detailed features will not be robust, particularly if based on inferences older than ~50 Ma. However, such reconstructions still provide valuable guidance as to the kinds of fluctuations in plate tectonic activity that are consistent with available constraints.

We define a reduced χ^2 misfit measure between predicted and “mapped” age distributions (e.g. from M08) as

$$\chi^2(t) = \sum_{i=0}^N \left(\frac{\alpha_{\text{model}}(\tau_i, t) - \alpha_{\text{map}}(\tau_i, t)}{\sigma_i} \right)^2 \quad (16)$$

where $\tau_i = i\Delta\tau$, $N = 150 \text{ Myr}/\Delta\tau$, and the bin size $\Delta\tau = 5 \text{ Myr}$. The uncertainties, σ_i , are those based on σ_s of Eq. (15) as shown in Fig. 2. We also consider a weighted misfit

$$\chi_w^2(t) = \frac{1}{\sum \alpha_{\text{map}}(\tau_i, t)} \sum_{i=0}^N \alpha_{\text{map}}(\tau_i, t) \left(\frac{\alpha_{\text{model}}(\tau_i, t) - \alpha_{\text{map}}(\tau_i, t)}{\sigma_i} \right)^2 \quad (17)$$

in order to account for the relatively larger amount of seafloor area that corresponds to the younger parts of the α curve. Lastly, we define a simple RMS misfit

$$\Delta\alpha(t) = \left(\frac{1}{N+1} \sum_{i=0}^N (\alpha_{\text{Model}}(\tau_i, t) - \alpha_{\text{map}}(\tau_i, t))^2 \right)^{1/2} \quad (18)$$

that does not take error estimates into account.

4. Results

4.1. Steady-state seafloor age distributions

For consistency with the time-dependent models which are discussed below, we always use a seafloor production rate that is based on extrapolating area per age curves, $\alpha(\tau, t)$ as in Fig. 2, to zero age where $C(t) = \alpha(\tau=0, t)$. For the present-day triangular distribution for the ϕ_t subduction probability, we obtain best-fit values $C_0 = 3.0 \text{ km}^2/\text{yr}$ and $\tau_m = 186 \text{ Ma}$ from Eq. (1). If we directly fit the triangular steady-state, α_t^s , distribution to $\alpha(t=0)$ from M08, we

Table 1

Misfit of steady-state area per age distribution, α^{ss} , for constant seafloor production rate, $C=C_0$, and the subduction models of Section 2 (cf. Fig. 1b)

Model		M08			C&H		
		χ^2	χ_w^2	$\Delta\alpha$ [km ² /Myr]	χ^2	χ_w^2	$\Delta\alpha$ [km ² /Myr]
Triangular	ϕ_t	4.8	6.9	0.13	8.3	6.9	0.26
Sqrt(age)	ϕ_s	4.6	5.6	0.18	17.4	15.8	0.24
Müller	ϕ_m	5.7	6.4	0.20	21.7	19.2	0.28
Uniform	ϕ_u	23.6	29.8	0.35	29.2	26.5	0.28
Bending	ϕ_b	24.8	25.2	0.40	53.4	48.1	0.33

We compute χ^2 misfit values taking into account errors (χ_w^2 is weighted by area, Eq. (17)) as well as mean deviation, $\Delta\alpha$ (Eq. (18)), for the present-day area per age distribution $\alpha(\tau, t=0)$ from M08 and Cogne and Humler (2004) (C&H).

obtain $C'_0=3.12\pm 0.07$ km²/yr and $\tau'_m=179\pm 5$ Myr, restricting the fit to $\tau\leq 150$ Ma for consistency with our misfit analysis below. This C'_0 is slightly larger than earlier, more detailed estimates for different seafloor age maps (Rowley, 2002; Cogne and Humler, 2004). However, our arguments are general, and the exact best-fit values are less important than the general comparison between different models. Also, the misfit for C_0 , $\chi^2=4.8$, is close to that for C'_0 , $\chi^2=4.5$.

Table 1 shows the misfits of the steady-state α^{ss} curves with M08 for the present-day and fixed C_0 . The triangular and sqrt(age) subduction probability models lead to the smallest misfit, with $\chi^2\sim 4.7$ for M08. Model ϕ_m leads to a larger misfit, and the uniform

and bending probabilities lead to very poor performance. If we repeat the analysis for the age distribution from Cogne and Humler (2004) (Table 1), we also find that ϕ_t and ϕ_s lead to best results, though ϕ_t fits the α curve now dramatically better in terms of χ^2 , while ϕ_s had slightly outperformed ϕ_t for M08. Comparing the χ^2 misfit estimate with the $\Delta\alpha$ deviations, the model performance is more consistent between the two α^{ss} estimates. Another discrepancy arises because Cogne and Humler (2004) inferred α by dividing the preserved seafloor area between isochrons by their temporal spacing (Sclater et al., 1981). This leads to a more jagged curve (Fig. 1b) because α is not allowed to change between isochrons. The difference in χ^2 misfit in Table 1 is thus partly due to features such as the α plateau around $\tau\sim 100$ Myr (Fig. 1b) which is best-fit by the triangular probability, ϕ_t , for χ^2 . Given that we have to base our analysis of seafloor ages for the past on M08, we use the χ^2 metric in the remainder.

Confirming earlier work (Rowley, 2002), the triangular distribution provides a good description of the present-day seafloor ages for constant production rate C_0 , although the sqrt(age), ϕ_s , model leads to similar performance for χ^2 . (The best-fitting C_0 for ϕ_s , 3.08 km²/yr, is very close to the general C_0 used above, and reduces χ^2 only insignificantly.) The finding that χ^2 misfits are close for α_t^{ss} and α_s^{ss} , but that χ_w^2 is smaller for α_s^{ss} than for α_t^{ss} means that the younger ages are fit better by the ϕ_s model. As noted, comparisons of small χ^2 differences are sensitive to analysis choices such as for uncertainties and should not be over-interpreted. Uniform α_u^{ss} and bending α_b^{ss} perform, however, consistently poorly for the present-day. It is

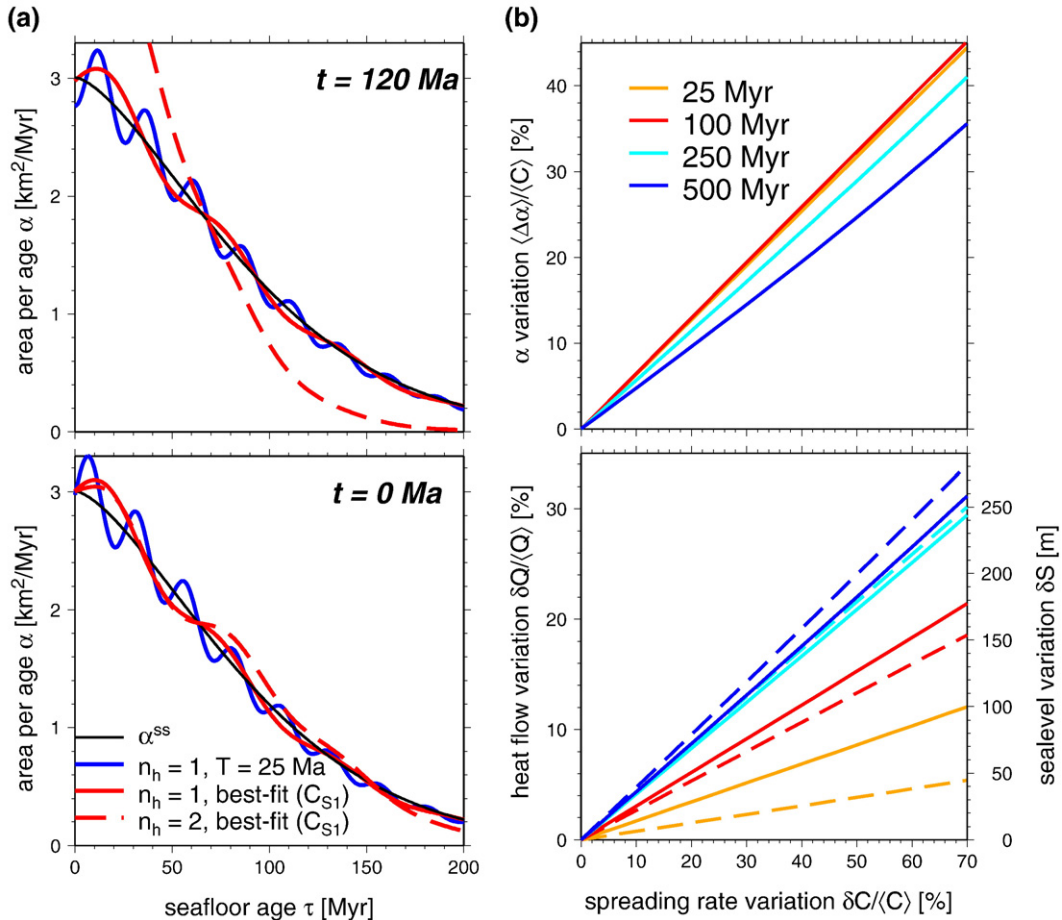


Fig. 3. (a) Predicted area per age, α , for sqrt(age) subduction models with constant C_0 (α^{ss}) and time-variable production rates $C(t)$, for two snapshots (left, top and bottom panels). We show a $n_h=1$ example with amplitude $A_1=10\%$ and period $T_1=25$ Myr (Eq. (7)) and best-fit models C_{S1} (Table 2). (b) Effect of single harmonic variations in C . Top: RMS deviation of $\alpha(t)$ from α^{ss} time-averaged over T , $\langle\Delta\alpha\rangle$, relative to mean production rate, $\langle C\rangle$, as a function of standard deviation of $C(t)$, δC , relative to $\langle C\rangle$. Bottom: Variation in oceanic heat flow, δQ , relative to mean (solid lines) and variation in sealevel, δS (dashed lines), as a function of δC . Colors indicate the period at which the C variations apply.

possible that different choices for k_4/k_3 for ϕ_b may improve performance closer to ϕ_m , and $\phi_b \rightarrow \phi_s$ for the case of weak bending.

4.2. Synthetic variations in seafloor production rate

The typical $\Delta\alpha$ deviations of the steady-state area per age distributions from M08 are ~ 0.2 km²/yr (Table 1), or $\sim 7\%$ of the seafloor production rate. It is clear that the complexities of plate tectonics, e.g. initiation or termination of spreading centers, are the cause of some of these deviations. Our model cannot capture such events, but it is instructive to explore how temporal variations in the seafloor production rate are mapped into age distributions. We use what we consider to be the simplest of our models, the sqrt(age) subduction probability, as an example for ϕ .

Fig. 3a shows age distributions, $\alpha(t)$, for time-dependent production rate, $C(t)$, scenarios including one where a single harmonic variation ($n_h=1$) with period $T=25$ Myr and amplitude $A\sim 10\%$ (Eq. (7)) is applied to roughly match Fig. 1b. Time-dependent computations are run from max(500,3T) Ma forward to remove the effect of the initial condition. Production rate fluctuations lead to a remnant signal in seafloor ages at damped amplitudes for old ages, $\tau \rightarrow \infty$. The time-averaged RMS variation $\langle \Delta\alpha \rangle$ between $\alpha(t)$ and α_s^s (computed in analogy to Eq. (18), but over one T time interval) scales roughly linearly with the amplitude of C fluctuation (top of Fig. 3b) and decreases slightly with increasing T ($C(t) \rightarrow C_0$ for $T \rightarrow \infty$). Fig. 3b also shows what kinds of variations in heat flow, δQ , and sealevel, δS , can be expected from single period variations in C (δ denotes standard deviation). Longer period fluctuations ($T/\tau_m > 1$) are most efficient in inducing significant δS and δQ because they can affect a wider range of seafloor age in a consistent fashion. Heat flow δQ variations are less than \sim half of the relative δC , and sealevel $\delta S \sim 200$ m for δC variability of 50% at T 200 Myr. Other choices for the subduction model such as ϕ_b or ϕ_m lead to similar behavior, with δS and δQ being different from the ϕ_s estimates only by $\sim 20\%$.

The remnant signature of production rate variability indicates that seafloor age can be used to explore the degree of spreading rate fluctuations in time-variable scenarios, for some limited duration back in time as permitted by the preserved seafloor. Fig. 3a shows model C_{S1} that was optimized for present-day area per age misfit, χ^2 , and allows for two harmonic variations (Table 2). Particularly for models that only use the present-day α , such optimizations suffer from large non-uniqueness due to trade-offs between model parameters; “best-fit” models should only be considered as representative of a whole class of solutions. However, the misfit for C_{S1} based on ϕ_s can be dramatically reduced, outperforming all ϕ models for constant production (Table 1), albeit using a larger number of degrees of freedom. Even with a single harmonic, the misfit can be reduced to $\chi^2 \sim 3.0$ for ϕ_s (Table 2). The physically motivated, sqrt(age) subduction probability model plus some moderate variability in production rates therefore provides an example of an alternative interpretation of the observed seafloor age distribution (cf. Demicco, 2004). Based on

Table 2

Model parameters (periods T and amplitudes A as of Eq. (7)) and misfits with M08 for harmonic production rate, C , models

Name	κ	n_h	T_1/T_2 [Myr]	$A_0/A_1/A_2$ [%]	χ^2 (χ_w^2)	$\langle \chi^2 \rangle$ ($\langle \chi_w^2 \rangle$)
C_{S1}	0	1	61	102/6	3.0(2.8)	4.6(5.6)
		2	357/62	140/40/7	1.9(2.1)	2.6(2.3)
C_{S2}	3	1	335	140/43	5.3(7.4)	2.3(2.0)
		2	274/131	114/50/31	1.8(2.0)	1.3(1.4)
C_{S3}	50	1	250	140/46	9.8(12.7)	1.8(1.6)
		2	213/119	130/48/27	2.4(2.7)	1.2(1.3)

C_{S1} , C_{S3} , and C_{S2} were optimized for the present-day area per age α ($\kappa=0$), time-averaged α ($\kappa=50$), and a joint measure of the two ($\kappa=3$, with the cost function for minimization $\chi^2 + \kappa \langle \chi_w^2 \rangle$), respectively. Here, χ^2 and $\langle \chi_w^2 \rangle$ denote α misfit (Eqs. (16) and (17)) for the present-day, and when time-averaged over the last 140 Ma, respectively.

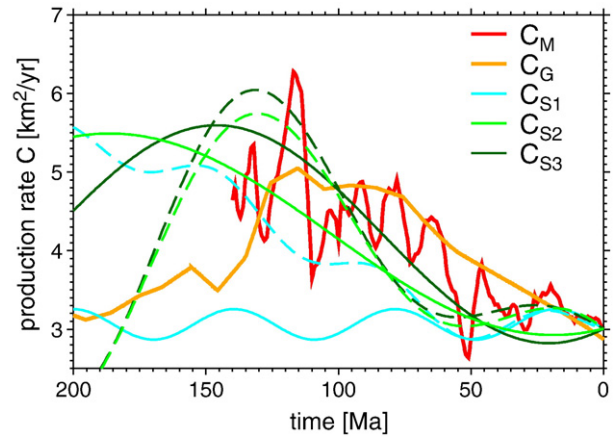


Fig. 4. Temporal variability in seafloor production rates, C , for the M08 paleo ages (C_M , mean $\pm \sqrt{2}$ standard deviation $\langle C_M \rangle = 3.27 \pm 10\%$ km²/yr for 60 Ma, and $\langle C_M \rangle = 4.04 \pm 28\%$ km²/yr for 140 Ma) and Gaffin's (1987) sealevel interpretation (C_G , $\langle C_G \rangle = 3.49 \pm 14\%$ km²/yr for 60 Ma, and $\langle C_G \rangle = 4.15 \pm 23\%$ km²/yr for 140 Ma). In addition, we show the best-fit synthetics from Table 2, solid and dashed curves are the $n_h=1$ and 2 alternatives, respectively.

the present-day α , we infer a signature of a ~ 60 Myr variability, with a hint of a longer period decrease of seafloor production rates (Fig. 4).

4.3. Geologically constrained variations in spreading rate

Fig. 2 shows how area per age distributions change over time based on the M08 reconstructions. While details of the distributions, such as the strong peak at $\alpha(\tau=30$ Myr, $t=140$ Ma) may not be robust, broad changes in α over time are expected to be associated with plate reconfigurations. Starting from an α distribution at 140 Ma that is smooth and similar to the present-day (except for the 30 Myr peak), plates evolve to 110 Ma, which stands out with a near-rectangular α distribution (Fig. 2). This type of α would be expected for a simple convective system (Parsons, 1982; Labrosse and Jaupart, 2007), and is mainly due to relatively equally-sized plates within the Pacific and Tethys (Müller et al., 2008b). By 60 Ma, the Izanagi plate and the Tethys have been subducted almost completely, and the Pacific plate itself has grown larger, with correspondingly more old seafloor that contributes to α . The amount of ridge-proximal, young seafloor then further decreases in the Pacific to the present-day (Lloyd et al., 2007), returning to a more triangular distribution. Assuming that the M08 reconstructions are at least approximately correct, Fig. 2 implies that the oceanic plates evolve over time; the present, triangularly-shaped α may be only representative for a limited duration.

We next compare seafloor production as inferred from the M08 age distributions by extrapolation of α to $C(t) = \alpha(\tau=0, t)$, C_M , with an older, independent estimate by Gaffin (1987) (Fig. 4), C_G . Gaffin assumed that the long-term sealevel variations for the last 395 Ma can be determined from the sealevel curves of Vail et al. (1977) and solved for C_G assuming that the sealevel fluctuations are caused by seafloor production rate variations alone. As mentioned, such curves are debated and corrections due to dynamic topography uncertain. However, Vail et al.'s curve is broadly consistent with newer estimates, the bathymetry inferred from paleo-ages for the last 60 Ma (Xu et al., 2006), and Müller et al.'s model for 140 Ma paleo-ages and dynamic topography for a convecting mantle (Müller et al., 2008b).

Fig. 4 shows the different estimates of paleo-seafloor production rates and quotes variabilities of $C(t)$ scaled up ($\sqrt{2}$ times standard deviation) to A_i amplitudes as in Eq. (7). C_G forms an upper envelope of C_M up to ~ 110 Ma where the curves diverge somewhat; C_M also has more detail than C_G , by design. For the last 60 Ma, we can also compute $C(t)$ from Xu et al. (2006) (not shown) and the oscillations in C_M with two local minima at ~ 30 and 50 Ma are confirmed. Overall,

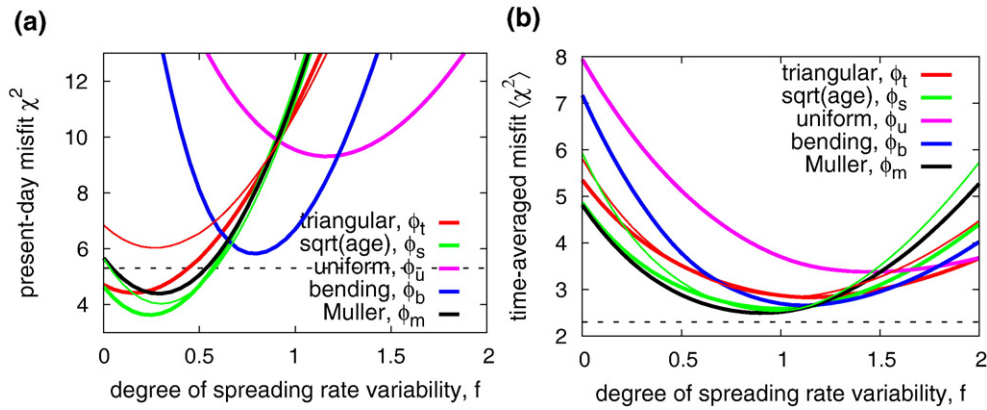


Fig. 5. (a) Misfit between predicted and mapped present-day area per age, α , as a function of variability in seafloor production rate, C (Eq. (19)), for different subduction probabilities and C_M variations. Heavy and thin lines (only shown for sqrt(age), ϕ_s , and Muller, ϕ_m), indicate regular, χ^2 , and area-weighted, χ_w^2 , misfit metrics, respectively. (b) Time-averaged misfit for α over 140 Ma. Dashed horizontal lines indicate the misfit of the $n_h=1$ C_{S2} best-fit synthetic (Table 2).

estimates for seafloor production rate variability agree in that there is $\sim 12\%$ and $\sim 25\%$ variability for the last 60 and 140 Ma, respectively, and that production rates were likely higher by $\sim 60\%$ at ~ 120 Ma.

4.4. Application to seafloor age distributions

We proceed to test if the geologically based spreading variability, in conjunction with our age evolution model, leads to an improvement in the fit to the present-day seafloor ages, as could be expected given the results from the synthetic variations. We treat the degree of spreading variation as adjustable via the parameter f

$$C(t, f) = C_0 + f(C_i(t) - C_0), \quad (19)$$

where $i=M$ or G , such that $f=0$ recovers the steady-state case of Fig. 1b, and $f=1$ is the original variability as in Fig. 4. Numerically, seafloor area per age is initialized with the steady-state solution for each subduction model before $C(t)$ applies from 140 Ma or 395 Ma onward for C_M and C_G , respectively. We compute the geometric average of the time-dependent misfit, $\langle \chi^2 \rangle$, referenced to the paleo α distributions inferred from M08 (Fig. 2), and χ^2 for the present-day as above.

Fig. 5a quantifies the model match to present-day α for time-variable C . Adding seafloor production rate variability at $f \sim 0.2$ – 0.4 from C_M improves the fit for the sqrt(age), ϕ_s , model, and some lesser variability improves the triangular ϕ_t model slightly. Variable C_M performance for the present day ϕ_s as in Fig. 5a leads to slightly poorer misfits than the $n_h=1$ synthetic C_{S1} , and significantly worse than the $n_h=2$ case (Table 2). The ϕ_b model, which approximates the effect of slab bending, requires larger variability, $f \sim 0.6$ – 0.9 , i.e. of order of C_M , to get closer to the best-performing ϕ_s model. Model ϕ_u cannot be improved beyond $\chi^2 \sim 10$, however, and the ϕ_m model leads to comparable performance to ϕ_s or ϕ_t .

Fig. 5b shows results for the time-averaged misfit; the area-weighted $\langle \chi_w^2 \rangle$ is consistently larger than $\langle \chi^2 \rangle$ for ϕ_m and ϕ_s . This indicates that the simple evolution model with $C(t)$ cannot reproduce the details of young seafloor generation. The 1-D model does, however, provide an adequate description of the overall evolution, and misfits are lowest for $f \sim 0.7$ – 1.1 in Fig. 5b. Those are the seafloor production rates that are consistent with the actual α from M08 against which $\langle \chi^2 \rangle$ is measured. The reduction of misfit by the addition of time-variable C is larger than the variations between different subduction models. We also find that ϕ_m , which is based on the M08 α curves themselves, leads to the best performance. The misfit for the simpler ϕ_s model is, however, almost as good as for ϕ_m . Comparing the other models, the time-variable performance is slightly better for sqrt(age) than for the triangular ϕ_t with constant τ_m which leads to $\langle \chi^2 \rangle$ values that are comparable to the bending

model ϕ_b at $f \sim 1.25$. Comparing the inferred model performance for C_G (not shown) with the misfits between model and M08 for C_M as in Fig. 5b, misfit minima are shifted to $f \sim 0.7$ for most ϕ models, and overall misfits are larger by ~ 1 for $\langle \chi^2 \rangle$. However, the relative model performance is similar.

An interesting solution that reduces both the present-day and time-variable misfits for geologically constrained seafloor production rates is ϕ_b . The bending model never leads to as good a fit as ϕ_s for present-day α , but to fairly good performance for $f \sim 0.8$, and ϕ_b is almost as good as ϕ_s for $\langle \chi^2 \rangle$, outperforming ϕ_t for $f \sim 1.2$ (Fig. 5). Given that regional subduction dynamics may strongly affect the overall role of bending, it is plausible that a model that lies between the ϕ_s and ϕ_b cases may lead to good performance for both the present-day, and the time-averaged match to α for spreading rate variations.

Using the sqrt(age), ϕ_s , model, we also inverted for best-fit synthetics that are optimized with a bias for time-averaged $\langle \chi^2 \rangle$ misfits. If we are mainly interested in long-term trends, and assuming that M08 is correct, it would be best to weigh $\langle \chi^2 \rangle$ much more than the present-day χ^2 . However, paleo-ages are also more uncertain which is why we show two synthetics in Table 2 to illustrate the differences from C_{S1} which was optimized for the present-day age distribution. C_{S2} and C_{S3} weigh $\langle \chi^2 \rangle$ 3 and 50 times more than χ^2 , respectively, and the intermediate C_{S2} performance for a single harmonic is also shown in Fig. 5. The best-fit harmonics predict $C(t)$ fluctuations that are broadly consistent with C_M and C_G (Fig. 4) in terms of periodicity and phase, and even the intermediate C_{S2} with a single $T \sim 340$ Myr, large amplitude fluctuation, performs slightly better for $\langle \chi^2 \rangle$ than every C_M model in Fig. 5b. Using two harmonics, the misfit can be further reduced and the best-fit periods are at ~ 130 Myr and a ~ 270 Myr “overtone” for C_{S2} (Fig. 4). The broad, sinusoidal decrease in seafloor production rates with ~ 250 Myr period, as inferred from the single period C_{S3} model, is required to fit the time-evolution of seafloor age based on M08.

5. Discussion

5.1. Oceanic plate tectonics

The present-day seafloor age distribution is well explained by simple, physically motivated evolution models and long-term variations in seafloor production rates. Synthetics and geologically reconstructed production curves (Fig. 4) indicate that there was a ~ 25 – 50% decrease in seafloor production since ~ 120 Ma, and the long-term cyclicity with ~ 250 Myr period broadly captures the more detailed evolution in M08 for the last 140 Ma. These variations in C rates affect the seafloor age distributions (Fig. 2), global heat flow (Harrison, 1980; Loyd et al., 2007), and sealevel (Müller et al., 2008b).

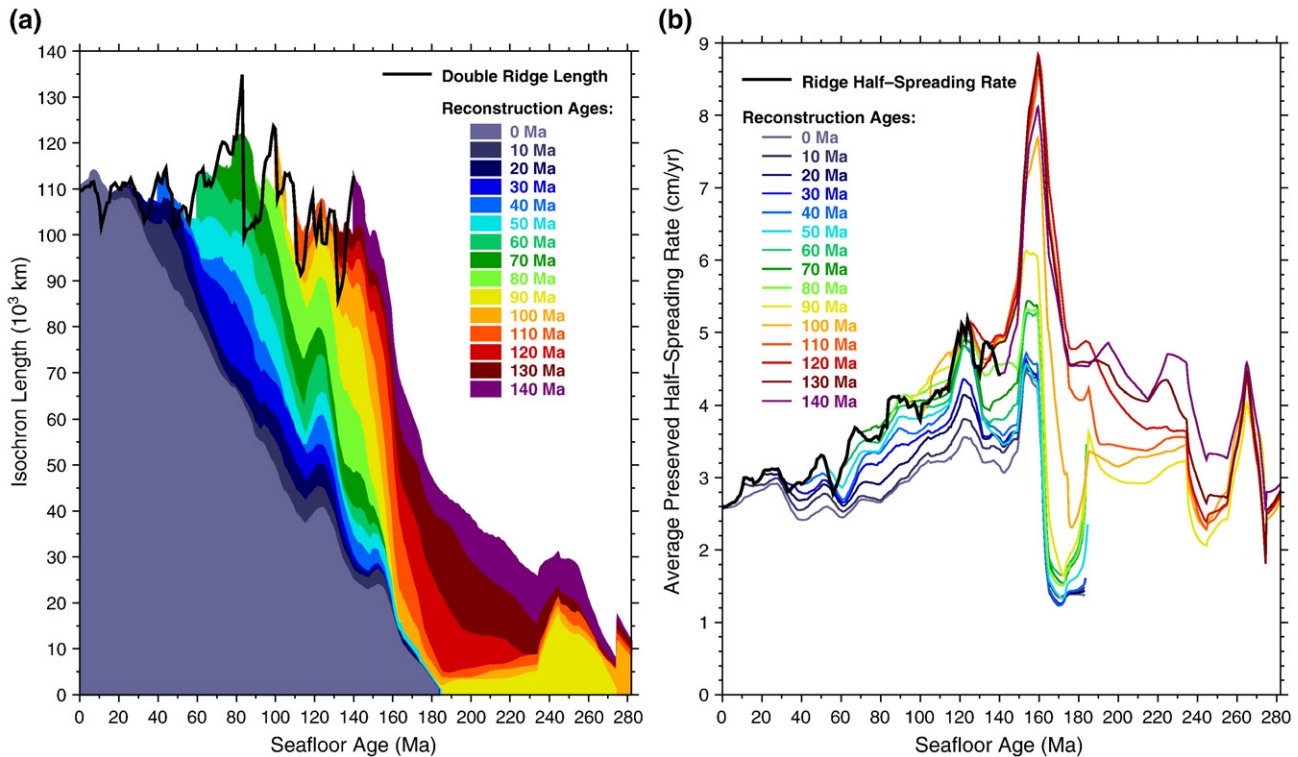


Fig. 6. Time-dependence of isochron length (a) and average preserved half spreading-rate (b), as determined from the M08 maps of reconstructed seafloor age back to 140 Ma. Black lines show the variation for the 0 Myr isochron, which is located at the ridge. Thus, the black lines show the double ridge length (a) and the half-spreading rate (b), as a function of time. Colored regions in (a) show the lengths of isochrons of a given seafloor age on individual M08 reconstructed seafloor age maps. Colored lines in (b) show the average half-spreading rate associated with those isochrons. Note that seafloor ages greater than 180 Ma (the age of the currently oldest seafloor) arise because the M08 reconstructions contain seafloor that formed earlier than 180 Myr ago but has since been subducted.

It is therefore interesting to further analyze the origin of the seafloor production variations based on M08.

The rate of seafloor production is given by the length of the 0 Myr isochron (which is double the ridge length) multiplied by the average half-spreading rate measured along the ridge. We calculate these quantities as a function of time (Fig. 6, black curves) by applying the method of Conrad and Lithgow-Bertelloni (2007) to seafloor younger than 5 Myr in the M08 age grids. We compare the variation in these quantities to those recorded by isochrons on individual M08 maps of reconstructed seafloor (colors in Fig. 6, determined using a 10 Myr averaging window). Colors in Fig. 6 refer to individual M08 reconstructions, and the x-axis refers to the time of seafloor formation. For example, M08's 90 Ma paleo-age map features seafloor with ages ranging from 0 Ma to ~185 Myr. This seafloor was formed between 90 and 275 Myr ago, and shows up between these ages in Fig. 6 (yellow curves). Estimates in Fig. 6 are, of course, subject to uncertainties associated with M08, especially those that may arise from the reconstruction of ridges and exhumation of subducted seafloor. Our use of a 10 Myr age window for calculating average values (one 5 Myr side of which is employed at ridges) tends to diminish these gridding issues and stabilize the curves in Fig. 6 compared to smaller averaging windows, while still maintaining their basic character.

While the seafloor production rate has dropped by ~55% since 140 Ma (Fig. 4), the spreading ridge length (Fig. 6a, black curves) has not changed much over the same time. There are intermittent peaks in length (e.g. at 80 Ma), but the general trend since 100 Ma is a moderate, ~16% decrease. Fig. 6b shows that the majority of the decrease in production rate is instead made up by variations in spreading rate. On average, those have decreased by ~45% since 140 Ma to ~2.6 cm/yr at present. This spreading rate slowdown, while a direct result of the M08 reconstruction, can not be detected solely from an analysis of the present-day seafloor (Rowley, 2002). This is because the seafloor that

was created at fast-spreading ridges has been preferentially subducted; this is apparent in the general broadening of the age distribution that has occurred since 140 Ma (Fig. 2), and also by the fact that the average spreading rate determined from seafloor that has survived subduction (colored lines in Fig. 6b) is systematically slower than the average spreading rate measured at the ridge (black line in Fig. 6b). The preferential destruction of young material is also apparent in the $\sqrt{\text{age}}$ probability relative to the triangular probability distribution (Fig. 1).

The finding that decreasing spreading rate, and not ridge length, dominated the Cretaceous seafloor production slowdown is slightly different from what Loyd et al. (2007) suggested from an analysis of the Pacific system. They showed that decreasing Pacific basin spreading length lead to a decrease in ridge-proximal area, and hence heat flow, toward the present. The M08 maps confirm this trend in the Pacific since the Cretaceous, but the small decrease in net ridge length (Fig. 6a) requires that shortening of the Pacific ridge system was largely compensated by lengthening of the Atlantic system. The major decrease in global average spreading rate (Fig. 6b) is consistent with the replacement of fast-spreading Pacific ridges by the slow-spreading Atlantic ridge in the global system. Thus, the M08 maps suggest that the net decrease in the rate of seafloor production since the mid-Cretaceous was primarily caused by a decrease in the globally averaged rate of seafloor spreading (Fig. 6). Although Loyd et al.'s (2007) explanation correctly represented the ridge-length decrease for the Pacific system, this trend was accompanied by growth of the slow-spreading Atlantic system that led to a dominance of spreading rate changes, and not ridge length, on the seafloor production rate.

5.2. Heat flow variability

One of the tectonic implications of the fluctuations in seafloor age distributions is the associated heat flow variability. Temporal

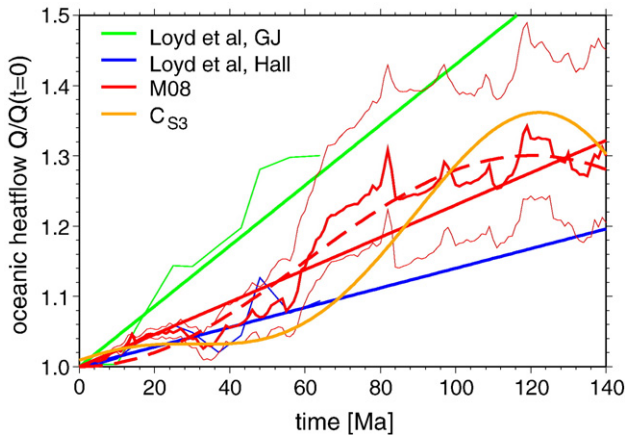


Fig. 7. Variation in oceanic heat flow relative to the present-day. We show two end-member estimates from Loyd et al. (2007), heat flow based on integration of M08 paleo ages (heavy line, method follows Loyd et al., 2007) with the min/max error estimates from Eq. (15) (thin lines), and the inferred heat flow from the $n_H=2$ synthetic C_{53} variations based on modeling area per age distributions. The best-fit linear curve for M08 has a slope of $-0.24\%/Myr$, and the dashed line indicates a cosine fit with period of 240 Myr.

variations in heat flow are important constraints for the thermal evolution of the Earth as described, for example, by parameterized convection models. Such models are potentially oversimplified and it might not be possible to find a complete, time-averaged description of all convective processes. However, a refined parameterized description of plate tectonics should still provide first-order insights into evolutionary behavior. A key parameter for such models is the Urey ratio between radiogenically generated and total convective heat transport. For low Urey ratios of ~ 0.3 at present, as inferred from cosmo-chemistry, the mantle is inferred to be too hot in the Archean if classical heat transport scalings are not modified (e.g. Korenaga, 2008). Alternatively, if oceanic heat flow were in a temporary high at present, the long-term Urey ratio may be underestimated, and no modification of the heat flow-Rayleigh number scaling would be required (Grigné et al., 2005). However, Loyd et al. (2007) found that heat flow is instead at a relative low at present, which means that the Urey ratio based on present-day heat flow may in fact be an over-estimate.

We can use the M08 paleo-ages and our synthetic production curves to compute oceanic heat flow from the changes in age distributions. Fig. 7 compares Q when computed from direct integration of paleo ages from M08 with Q as inferred from the best-fit C_{53} synthetic and integration of α . The estimated linear decrease in heat flow based on M08 integration is $-0.24\%/Myr$, and falls between the earlier estimates by Loyd et al. (2007) for 60 Ma. The sum of squares of residuals for the linear fit is 0.18 and can be reduced to 0.09 with a two parameter cosine that corresponds to a period of 240 Myr at 15% heat flow amplitude variation. This period is very close to the single harmonic C_{53} model (250 Myr, Table 2), and similar to the longer (~ 210 Myr) of the two harmonic models shown in Fig. 7. We interpret these findings such that there is evidence for a decrease in heat flow by ~ 10 – 25% since ~ 100 Ma, and that the rate of decrease might have slowed during the last ~ 50 Ma, as would be expected from cyclical behavior, rather than a linear trend.

6. Conclusions

An evolutionary model that incorporates subduction probabilities that are proportional to $\sqrt{\text{age}}$, i.e. slab pull, can provide a good description of the present-day seafloor area per age distribution. This is a viable alternative to the constant seafloor destruction-rate hypothesis that leads to the triangular distribution. The $\sqrt{\text{age}}$ probability provides an equivalent fit to the age distributions for constant seafloor

production, and this model outperforms the triangular model if spreading rate variations are allowed. The triangular distribution of seafloor ages at present may be only one of several, perhaps typical, stages that the oceanic plates evolve through while convective length scales self-adjust to the boundary conditions that continents impose. Models that are based on extrapolating the assumptions required to achieve a triangular distribution for the present-day may not provide a valid description of long-term dynamics.

Variations in heat flow based on recent paleo-age reconstructions back to 140 Ma are quantitatively consistent with the independent, earlier analysis by Loyd et al. (2007) for the last 60 Ma. The Earth's mantle is currently in a state of relatively low surface heat flux, and the last 140 Ma may be part of a long-term episodic behavior. This finding lends further support to relatively low estimates of average Urey ratios and emphasizes the need for improved heat transport scalings (e.g. Korenaga, 2008). Our modified $\sqrt{\text{age}}$ subduction probability model that additionally accounts for the effect of viscous bending of slabs is a candidate for a parameterized description of convective motions of the lithosphere. With the bending formulation, it may be possible to satisfy both the requirements of a ~ 1 -Gyr time-scale, modified heat transport law, and the ~ 100 Myr time-scale fluctuations in seafloor age distributions throughout the Wilson (1966) cycle.

The rates of decrease in heat flow and seafloor production have been slowing down over the last tens of Ma. If the variations are indeed cyclic, we might well be seeing typical variations throughout common oceanic and continental plate reorganizations. Heat flow and ridge length are then expected to increase again in the future, which would also imply that plate tectonics is not about to shut down as was suggested (Silver and Behn, 2008). A consistent picture arises where spreading rate, sealevel, and heat flow variations on several time-scales can be described in a common mechanical framework. Such a description of time-variable plate tectonics may provide crucial quantitative predictions if we want to understand the interplay between oceanic and continental plates and long-term Earth evolution.

Acknowledgments

We thank two anonymous reviewers for their comments which helped to clarify the presentation, Adam Maloof and Frederic Simons for discussions, and Dave Rowley for comments on triple junctions. Most figures were produced with GMT (Wessel and Smith, 1991). Part of this research was funded by NSF through grants EAR-0633879 and EAR-0643365 (TWB), and EAR-0609590 (CPC).

References

- Becker, T.W., Faccenna, C., O'Connell, R.J., Giardini, D., 1999. The development of slabs in the upper mantle: insight from numerical and laboratory experiments. *J. Geophys. Res.* 104, 15207–15225.
- Buffett, B.A., 2006. Plate force due to bending at subduction zones. *J. Geophys. Res.* 111. doi:10.1029/2006JB004295.
- Cogne, J.-P., Humler, E., 2004. Temporal variation of oceanic spreading and crustal production rates during the last 180 Myr. *Earth Planet. Sci. Lett.* 227, 427–439.
- Conrad, C.P., Hager, B.H., 1999. The effects of plate bending and fault strength at subduction zones on plate dynamics. *J. Geophys. Res.* 104, 17551–17571.
- Conrad, C.P., Lithgow-Bertelloni, C., 2007. Faster seafloor spreading and lithosphere production during the mid-Cenozoic. *Geology* 35, 29–32.
- Davies, G.F., 1992. On the emergence of plate tectonics. *Geology* 20, 963–966.
- Demicco, R.V., 2004. Modeling seafloor-spreading rates through time. *Geology* 32, 485–488.
- Engelbreton, D.C., Cox, A., Gordon, R.G., 1985. Relative motions between oceanic and continental plates in the Pacific basin. *Geol. Soc. Am. Spec. Paper*, vol. 206.
- Fiet, N., Quidelleur, X., Parize, O., Bulot, L.G., Gillot, P.Y., 2006. Lower Cretaceous stage durations combining radiometric data and orbital chronology: towards a more stable relative time scale? *Earth Planet. Sci. Lett.* 246, 407–417.
- Gaffin, S., 1987. Ridge volume dependence on seafloor generation rate and inversion using long term sealevel change. *Am. J. Sci.* 287, 596–611.
- Grigné, C., Labrosse, S., Tackley, P.J., 2005. Convective heat transfer as a function of wavelength. Implications for the cooling of the Earth. *J. Geophys. Res.* 110. doi:10.1029/2004JB00376.
- Gurnis, M., 1990. Ridge spreading, subduction, and sea level fluctuations. *Science* 250, 970–972.

- Hardie, L.A., 1996. Secular variation in seawater chemistry: an explanation for the coupled secular variation in the mineralogies of marine limestones and potash evaporates over the past 600 m.y. *Geology* 24, 279–283.
- Harrison, C.G.A., 1980. Spreading rates and heat flow. *Geophys. Res. Lett.* 7, 1041–1044.
- Hays, J.D., Pitman III, W.C., 1973. Lithospheric plate motion, sea level changes, and climatic and ecological consequences. *Nature* 246, 18–22.
- Heller, P.L., Anderson, D.L., Angevine, C.L., 1996. Cretaceous pulse of rapid seafloor spreading: real or necessary? *Geology* 24, 491–494.
- Jaupart, C., Labrosse, S., Marechal, J.-C., 2007. Temperatures, heat and energy in the mantle of the Earth. In: Schubert, G., Bercovici, D. (Eds.), *Treatise on Geophysics*. Elsevier, pp. 253–303.
- Korenaga, J., 2007. Eustasy, supercontinental insulation, and the temporal variability of terrestrial heat flux. *Earth Planet. Sci. Lett.* 257, 350–358.
- Korenaga, J., 2008. Urey ratio and the structure and evolution of Earth's mantle. *Rev. Geophys.* 46. doi:10.1029/2007RG000241.
- Labrosse, S., Jaupart, C., 2007. Thermal evolution of the Earth: secular changes and fluctuations of plate characteristics. *Earth Planet. Sci. Lett.* 260, 465–481.
- Larson, R.L., Pitman III, W.C., 1972. World-wide correlation of Mesozoic magnetic anomalies and its implications. *GSA Bull.* 83, 3645–3662.
- Lee, C.-T.A., Lenardic, A., Cooper, C.M., Niu, F., Levander, A., 2005. The role of chemical boundary layers in regulating the thickness of continental and oceanic thermal boundary layers. *Earth Planet. Sci. Lett.* 230, 379–395.
- Lithgow-Bertelloni, C., Gurnis, M., 1997. Cenozoic subsidence and uplift of continents from time-varying dynamic topography. *Geophys. Res. Lett.* 25, 735–738.
- Lithgow-Bertelloni, C., Richards, M.A., Ricard, Y., O'Connell, R.J., Engebretson, D.C., 1993. Toroidal–poloidal partitioning of plate motions since 120 Ma. *Geophys. Res. Lett.* 20, 375–378.
- Loyd, S.J., Becker, T.W., Conrad, C.P., Lithgow-Bertelloni, C., Corsetti, F., 2007. Time-variability in Cenozoic reconstructions of mantle heat flow: plate tectonic cycles and implications for Earth's thermal evolution. *Proc. Natl. Acad. Sci.* 104, 14,266–14,271.
- Müller, D., Roest, W.R., Royer, J.-Y., Gahagan, L.M., Sclater, J.G., 1997. Digital isochrons of the world's ocean floor. *J. Geophys. Res.* 102, 3211–3214.
- Müller, R.D., Sdrolias, M., Gaina, C., Roest, W.R., 2008a. Age, spreading rates and spreading asymmetry of the world's ocean crust. *Geochem. Geophys. Res.* 9. doi:10.1029/2007GC001743.
- Müller, R.D., Sdrolias, M., Gaina, C., Steinberger, B., Heine, C., 2008b. Long-term sea-level fluctuations driven by ocean basin dynamics. *Science* 319, 1357–1362.
- Nelder, J.A., Mead, R., 1965. A simplex method for function minimization. *Comput. J.* 7, 308–313.
- O'Connell, R.J., Gable, C.W., Hager, B.H., 1991. Toroidal–poloidal partitioning of lithospheric plate motions. In: Sabadini, R., Lambeck, K. (Eds.), *Glacial Isostasy, Sea-Level and Mantle Rheology*. Kluwer Academic Publishers, Norwell, MA, pp. 535–551.
- Olson, P., Bercovici, D., 1991. On the equipartitioning of kinematic energy in plate tectonics. *Geophys. Res. Lett.* 18, 1751–1754.
- Parsons, B., 1982. Causes and consequences of the relation between area and age of the ocean floor. *J. Geophys. Res.* 87, 289–302.
- Phillips, B.R., Bunge, H.-P., 2005. Heterogeneity and time dependence in 3D spherical mantle convection models with continental drift. *Earth Planet. Sci. Lett.* 233, 121–135.
- Pitman III, W.C., 1978. Relationship between eustasy and stratigraphic sequences of passive margins. *Geol. Soc. Amer. Bull.* 89, 1389–1403.
- Rowley, D.B., 2002. Rate of plate creation and destruction: 180 Ma to present. *GSA Bull.* 114, 927–933.
- Sclater, J.G., Parsons, B., Jaupart, C., 1981. Oceans and continents: similarities and differences in the mechanism of heat loss. *J. Geophys. Res.* 86, 11,535–11,552.
- Silver, P.G., Behn, M.D., 2008. Intermittent plate tectonics? *Science* 319, 85–88.
- Stein, C.A., Stein, S., 1992. A model for the global variations in oceanic depth and heat flow with lithospheric age. *Nature* 359, 123–129.
- Vail, P.R., Mitchum Jr., R.M., Todd, R.G., Widmier, J.M., Thompson, S., Sangree, J.B., Bubb, J.N., Hatlelid, W.G., 1977. Seismic stratigraphy and global changes of sea level. In: Payton, C.E. (Ed.), *Seismic stratigraphy – Applications to Hydrocarbon Exploration*. Amer. Assoc. Petrol. Geol. Mem., vol. 26. American Association of Petroleum Geologists, pp. 49–205.
- Walzer, U., Hendel, R., 2008. Mantle convection and evolution with growing continents. *J. Geophys. Res.* 113. doi:10.1029/2007B005459.
- Wessel, P., Smith, W.H.F., 1991. Free software helps map and display data. *Eos, Trans. – Am. Geophys. Union* 72, 445–446.
- Wilson, J.T., 1966. Did the Atlantic close and then reopen? *Nature* 211, 676–681.
- Xu, X., Lithgow-Bertelloni, C., Conrad, C.P., 2006. Reconstructions of Cenozoic seafloor ages: implications for sea level. *Earth Planet. Sci. Lett.* 243, 552–564.
- Zhong, S., Zhang, N., Li, Z.-X., Roberts, J.H., 2007. Supercontinent cycles, true polar wander, and very long wavelength mantle convection. *Earth Planet. Sci. Lett.* 261, 551–564.